

# Planar laser-induced incandescence of turbulent sooting flames: the influence of beam steering and signal trapping

Z. W. Sun<sup>1,2</sup> · Z. T. Alwahabi<sup>2,3</sup> · D. H. Gu<sup>1,2</sup> · S. M. Mahmoud<sup>1,2</sup> · G. J. Nathan<sup>1,2</sup> · B. B. Dally<sup>1,2</sup>

Received: 14 November 2014 / Accepted: 7 March 2015 / Published online: 25 March 2015  
© Springer-Verlag Berlin Heidelberg 2015

**Abstract** The influence of beam steering and signal trapping on the accuracy of soot volume fractions measured using planar laser-induced incandescence (LII) has been investigated in turbulent non-premixed sooting flames at atmospheric pressure. In turbulent non-premixed  $C_2H_4$ /air flames, the influence of local de-focusing/focusing of the laser sheet from beam steering can result in the underestimate of the averaged LII signal by 30 %, even when operating within the so-called plateau regime of laser fluence. Beam steering was also found to be significant in both the upstream region of  $C_2H_4$ /air flames and non-reacting  $C_2H_4$  flows, because the fuel has a relatively high refractive index compared with ambient air. The extent of beam steering at different heights of reacting and isothermal flows as well as its dependence on exit Reynolds number ( $Re$ ) has been measured. The measurements reveal that even at low turbulence levels ( $2000 < Re < 3000$ ), beam steering effects can be significant. Also found is that the LII signal at a 450 nm wavelength can be attenuated by a few per cent at high soot loading regions in turbulent flames due to signal trapping. Finally, the feasibility of directly evaluating the signal attenuation via planar LII results was assessed by

comparing the virtual soot attenuation calculated based on the planar LII result with that measured using light-of-sight extinction.

## 1 Introduction

Laser-induced incandescence (LII) is currently the state of the art in the quantitative measurements of soot volume fractions ( $f_v$ ) and is widely employed to advance understanding of the mechanisms that govern the evolution of soot in flames. Planar LII has many advantages over the laser extinction method because it can provide spatially and temporally resolved measurements of  $f_v$ , while extinction is limited to providing the integrated  $f_v$  over the beam path. These advantages are especially beneficial in turbulent flame measurements, where the distribution of soot sheets is spatially inhomogeneous and varies with time. To obtain reliable measurements of  $f_v$ , much effort has been made to improve the measurement accuracy of planar LII. For example, previous investigations have advanced understanding of the soot's physical and chemical properties [1–4], the LII process itself [5–8], and the calibration process used to quantify the LII signals [5, 9–11]. These studies have found that collecting the LII signal prompt with the infrared excitation beam at 1,064 nm can provide accurate measurements of  $f_v$  in laminar, non-elevated pressure flames. However, in turbulent flames additional effects, such as beam steering and signal trapping, can influence the measurement accuracy. Importantly, systematic investigation of influence of these two effects on LII measurements in turbulent flames has been rarely reported, even in flames at atmospheric pressure.

Beam steering is caused by gradient components of the refractive index normal to the beam propagation and is

---

**Electronic supplementary material** The online version of this article (doi:10.1007/s00340-015-6080-6) contains supplementary material, which is available to authorized users.

---

✉ Z. W. Sun  
zhiwei.sun@adelaide.edu.au

<sup>1</sup> School of Mechanical Engineering, The University of Adelaide, Adelaide, SA 5005, Australia

<sup>2</sup> Centre of Energy Technology, The University of Adelaide, Adelaide, SA 5005, Australia

<sup>3</sup> School of Chemical Engineering, The University of Adelaide, Adelaide, SA 5005, Australia

difficult to predict or avoid in turbulent flows and flames. These gradients change the direction of the beam and distort its spatial intensity profile. These changes can influence the signal intensity and/or the measurement accuracy of many commonly employed optical techniques, e.g. LII [10], laser-induced fluorescence (LIF) [12, 13], coherent anti-Stokes Raman scattering (CARS) [12, 14], particle image velocimetry (PIV) [15], Rayleigh scattering [16, 17], and other techniques that are based on line-of-sight attenuation [18, 19]. Hence, it is necessary to assess the influence of gradients in refractive index on measurement uncertainty in turbulent flows, especially for techniques that are sensitive to laser fluence, such as LII.

The influence of beam steering on LII measurements has rarely been reported even though the effect has been recognized widely for a long time. To date, the only related work was reported by Zerbs et al. [10], who investigated the changes in the local laser fluence and the beam pattern in turbulent sooting  $C_2H_4$ /air flames at different pressures from atmospheric to 9 bars. They found that the beam pattern changes dramatically from one shot to another and that the local fluence varies significantly from 30 to 200 % of the initial values. As a result, neither locally saturated laser fluence ( $>0.3 \text{ J/cm}^2$ ) nor a spatial resolution better than 1 mm can be guaranteed at the highest pressure (9 bars). Zerbs et al. also found that the changes to the beam pattern are worse for the high-pressure case. This finding is consistent with another study of beam steering effect on the CARS and LIF techniques applied in flames [12]. While there is some limited information on these effects at high-pressure combustion and non-reacting flow conditions, very little has been reported under atmospheric conditions. The authors have noted in a previous work that there is a tangible influence by beam steering on soot volume fraction measurements using the planar LII technique in turbulent sooting flames [20]. It was found that the averaged planar LII signal is asymmetric relative to the centreline of the turbulent jet flames at atmospheric pressure under study. The averaged LII signal on the beam-incident side was found to be stronger than that on the beam-exit side. The uneven signal cannot be explained by the attenuation of highly saturated laser fluence ( $\sim 1.0 \text{ J/cm}^2$ ) by soot particles. Asymmetric LII images, observed with symmetric averaged  $OH^*$  chemiluminescence, were also reported by Köhler et al. without providing any definite explanation [21]. The authors had performed planar LII, point-wise CARS and PIV measurements in non-premixed  $C_2H_4$ /air turbulent jet flames, with the same aim as the work reported in [20], to provide new and extensive data in turbulent sooting flames for soot model validation. A possible explanation for the asymmetric LII signals is the distortion of the laser sheet due to the influence of beam steering that occurred in the flames. To assess this proposition and provide more reliable experimental data for modelling, the

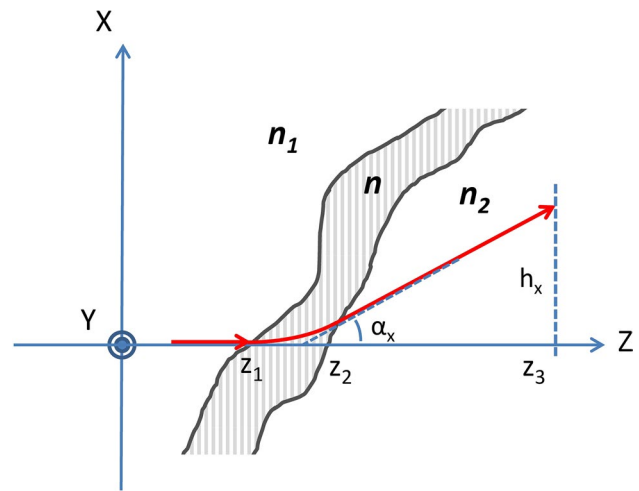


**Fig. 1** Refraction of a light ray, showing the deflection distance  $h_x$  caused by the mixture boundary of a dual-gas system

present paper reports the influence of beam steering on beam patterns passed through flames together with the planar LII signals recorded simultaneously in atmospheric sooting flames. It also aims to reveal the relationship between beam steering and LII signals at different exit Reynolds numbers ( $Re$ ), and hence different turbulence intensities.

Beam steering arises from the non-homogeneity of the refractive index ( $n$ ) field of the fluid medium. According to the Gladstone–Dale relation, the refractive index is the product of the Gladstone–Dale constant  $K$  and the fluid density  $\rho$ , which can be expressed as [22]

$$n(x, y, z) - 1 = K(x, y, z)\rho(x, y, z). \quad (1)$$

For a gas mixture containing  $m$  species, a more general expression can be written as

$$n(x, y, z) - 1 = \sum_{i=1}^m K_i(x, y, z)\rho_i(x, y, z), \quad (2)$$

where  $\rho_i$  are the partial densities of the individual components. For a simplified two-gas mixture system, as shown in Fig. 1, the deflection angle at  $x$  direction of a light ray crossing the mixing boundary,  $\alpha_x$ , can be expressed as [22]

$$tg(\alpha_x) \cong \int_{z_1}^{z_2} \frac{1}{n} \cdot \frac{\partial n}{\partial x} dz, \quad (3)$$

and the deflection distance  $h_x$  at the plane of  $z = z_3$  is

$$h_x \cong (z_3 - z_1) \cdot tg(\alpha_x). \quad (4)$$

For a gaseous system, the integration part of Eq. (3) can be rewritten as

$$\frac{1}{n} \cdot \frac{\partial n}{\partial x} \cong \frac{\partial n}{\partial x} = \frac{\partial(K \cdot \rho)}{\partial x} = \frac{P}{R} \left( \frac{1}{T} \frac{\partial K}{\partial x} - \frac{K}{T^2} \frac{\partial T}{\partial x} \right), \quad (5)$$

where  $P$  is the pressure,  $T$  is the gas temperature, and  $R$  is the gas constant. In the derivation of Eq. (5), the ideal gas law, i.e.  $\rho = P/RT$ , and an approximation of  $1/n = 1$  have been used. The deflection distance,  $h_x$ , is then rewritten as

$$h_x \cong (z_3 - z_1) \frac{P}{R} \int_{z_1}^{z_2} \left( \frac{1}{T} \frac{\partial K}{\partial x} - \frac{K}{T^2} \frac{\partial T}{\partial x} \right) dz, \quad (6)$$

Equation (6) reveals that the light deflection can be induced both by the change of gas composition and by the component of temperature gradient normal to the light propagation. The extent is dependent on the width of, and gradients through, the inhomogeneous region. This applies for conditions such as when a laser beam passes through the mixing boundary of two gases (even for cold flows at room temperatures) or a flame. Given that, in turbulent flows, the index of refraction is time dependent [i.e.  $n = n(x, y, z, t)$  where  $t$  denotes the time], such deflections are difficult to characterize. Therefore, new experimental data are needed to guide the development of methods with which to better account for the effects of beam distortion.

Signal trapping is another potential source of uncertainty for  $f_v$  measurements using LII, e.g. [23–25]. Incandescence signals emitted from the laser sheet plane are attenuated along the optical path to the detector. This attenuation can be caused by scattering and absorption of soot particles and also by absorption of soot precursors, such as polycyclic aromatic hydrocarbons (PAHs), in a broadband spectral region from the UV to 680 nm [26]. It has previously been suggested that LII measurements in flames employ signal detection at short wavelengths because the natural soot luminosity decreases sharply towards the UV [5]. However, LII signals at short wavelengths, for instance in the blue region  $\sim 450$  nm, are expected to be attenuated more significantly than those at long wavelengths in the red spectral region. This attenuation is not only due to PAH, but also because of the optical extinction caused by soot particles, which is inversely proportional to the beam wavelength  $\lambda$  in the visible spectral region [27]. Therefore, it is important to study and correct for the influence of signal trapping on LII measurements, especially in locations where soot loading is high, and short-wavelength LII signals are collected through a blue band-pass or interference filter. This applies to most studies, in which soot volume fractions were measured in non-premixed, sooting turbulent flames using LII. For example, an interference filter centred at  $450 \pm 10$  nm with a full-width-at-half-maximum (FWHM) of  $40 \pm 8$  nm was used by Köhler et al. [21, 28] in studying a lifted, non-premixed sooting  $C_2H_4$ /air flame; a band-pass filter centred at 430 nm (with a FWHM of 10 nm) was used by the Adelaide group to perform  $f_v$  measurements in attached sooting flames [20, 29]; a broad detection band of 300–600 nm for LII signals was used by Shaddix et al. [30] in similar studies. To quantify LII signal trapping at the wavelengths

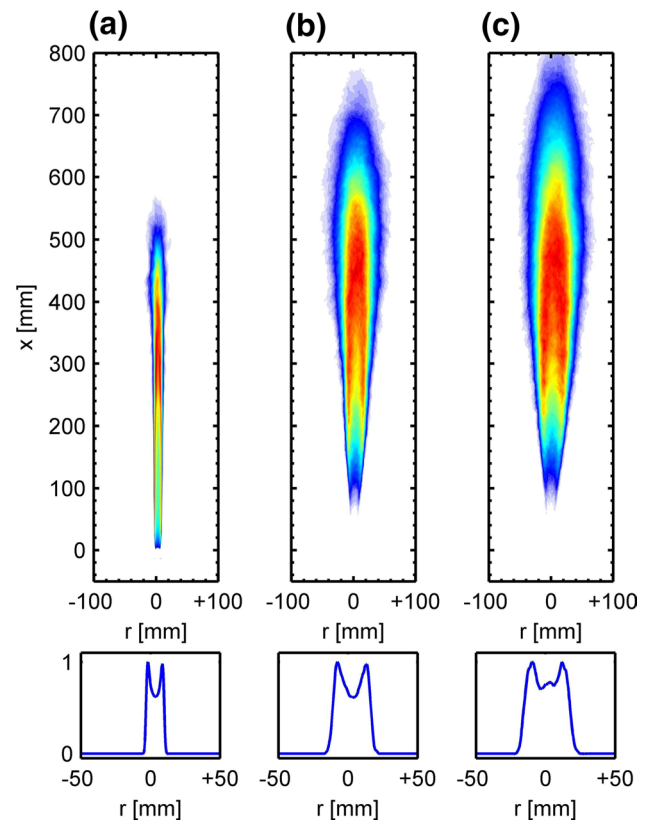


**Fig. 2** Soot luminosity around 700 nm recorded in three  $C_2H_4$ /air non-premixed flames with different Reynolds numbers of (a) 660, (b) 5240, and (c) 11,670. The corresponding cross sections (a) at  $x = 160$  mm, for (b) and (c) at  $x = 200$  mm are shown as well. The images are averaged over 300 instantaneous images recorded by a CCD camera mounted with a band-pass filter centred at 700 nm with a 40-nm transmission band. The fuel pipe ends at  $x = 0$  mm

typical of LII planar measurements, a 450-nm laser beam was employed in the present work to perform the extinction measurements in turbulent sooting flames. The extinction results were compared with the virtual attenuations calculated with soot volume fractions measured with planar LII to assess the feasibility of directly evaluating the magnitude of signal trapping in planar LII measurements.

## 2 Experimental set-up

### 2.1 Burner

A straight-pipe jet burner was employed in the present study for both the sooting flames and the non-reacting flows. A round aluminium tube, with an inner diameter ( $d$ ) of 4.4 mm, was mounted in the middle of a square contraction ( $150 \text{ mm} \times 150 \text{ mm}$ ), delivering co-flowing air at an ambient temperature and a mean velocity of 1.1 m/s. The fuel pipe has a length of 385 mm, including a tapered end

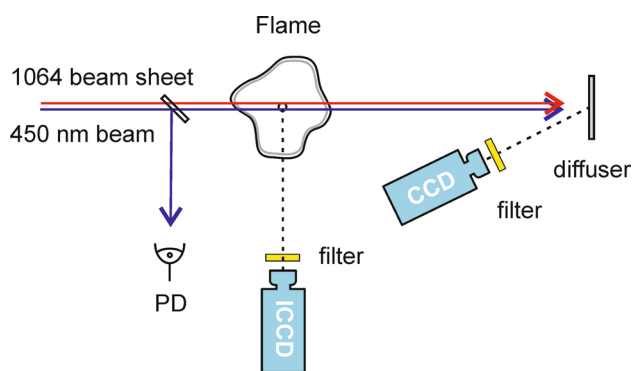


**Fig. 3** Schematic diagram of the experimental set-up. PD is a photodiode

at the jet outlet that was raised 18 mm above the contraction edge. A traverse was used to move the burner vertically to achieve measurements at different heights above the nozzle.

Figure 2 presents the luminosities of three non-premixed  $C_2H_4$ /air flames stabilized on this burner. The flames had different Reynolds numbers of 660, 5240, and 11,670 at the nozzle exit. The luminosity images were averaged over 300 instantaneous images recorded with a CCD camera (MegaPlus ES4020). A band-pass filter centred at 700 nm with a transmission band of 40 nm was mounted in front of the camera to only gather light emission in the IR regime. All three flames show good symmetry in soot luminosity about the flame centreline, which is demonstrated clearly by the cross sections of luminosity images in Fig. 2. When further increasing the fuel flow rate and  $Re > 11,670$ , the flame lifted from the burner nozzle. No investigation was performed in any lifted flames in the present work. These images show that there is no inherent asymmetry in the soot concentration in these flames.

## 2.2 Optics

Figure 3 presents a schematic diagram of the optical arrangement. The 1,064 nm output from a Nd:YAG laser (Brilliant B) was used to provide the light source for the LII measurements. The round laser beam was expanded via two cylindrical lenses ( $f = -40$  mm and  $f = 100$  mm) and then focused into a laser sheet via a cylindrical lens of  $f = 1,000$  mm. Before the first cylindrical lens ( $f = -40$  mm), no optics were applied to smooth the laser beam; only a combination of a half-wave plate and a Glan-laser polarizer was used to vary the laser power. The laser was operated at its maximum power output. The laser sheet had a height of  $\sim 20$  mm and was directed through the centreline of the jets or flames. An intensified CCD camera was mounted perpendicular to the laser sheet to collect

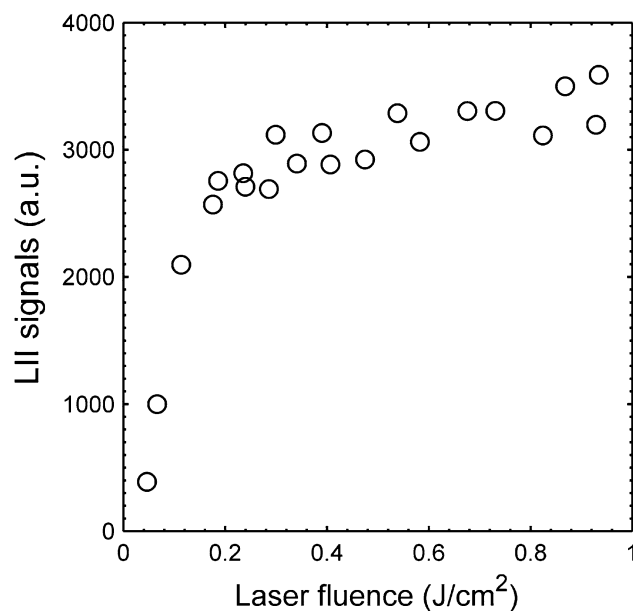


**Fig. 4** Prompt LII signal intensity as a function of laser fluence for the present optical arrangement

the prompt LII signal by setting the gate width to 40 ns. The camera was equipped with a band-pass filter centred at 450 nm (with a 10 nm FWHM) and a Nikon lens ( $f = 50$  mm and  $F/1.4$ ).

Figure 4 presents the fluence curve for the current set-up, which was used to assess the quality of the so-called plateau regime. The curve was measured in a premixed  $C_2H_4$ /air flat sooting flame (with an equivalence ratio  $\varphi = 2.0$ ), stabilized on a McKenna-type burner (Holthuis & Associates). A flame stabilizer, parallel to the burner surface, was located at a height of 20 mm above the burner surface (HAB). The measuring point was centred at 14 mm HAB. All results in Fig. 4 were averaged for 50 laser shots and for a  $10 \times 5$  mm<sup>2</sup> (width  $\times$  height) area. A 'plateau' regime, over which the LII signal was constant to within about  $\pm 9$  %, is generated at laser fluence  $> 0.3$  J/cm<sup>2</sup>. The fluence curve does not exhibit any peak, which is often found near to the start of the plateau region and is associated with the onset of soot sublimation. This implies that the laser beam provided by the multi-mode Nd:YAG laser has a poor Gaussian profile [31]. The 'constant' LII signals in Fig. 4, as for those in most planar LII measurements, are the averaged results of different laser fluence along the laser sheet thickness. The laser fluence used in the present work was around 0.8 J/cm<sup>2</sup>.

A flat glass diffuser ( $50 \times 50$  mm<sup>2</sup>) was mounted  $\sim 2.2$  m down-beam from the flame and aligned perpendicular to the laser beam. To record the spatial profiles of the laser sheet which passed through the flames, the diffused reflection was recorded by a CCD camera (MegaPlus

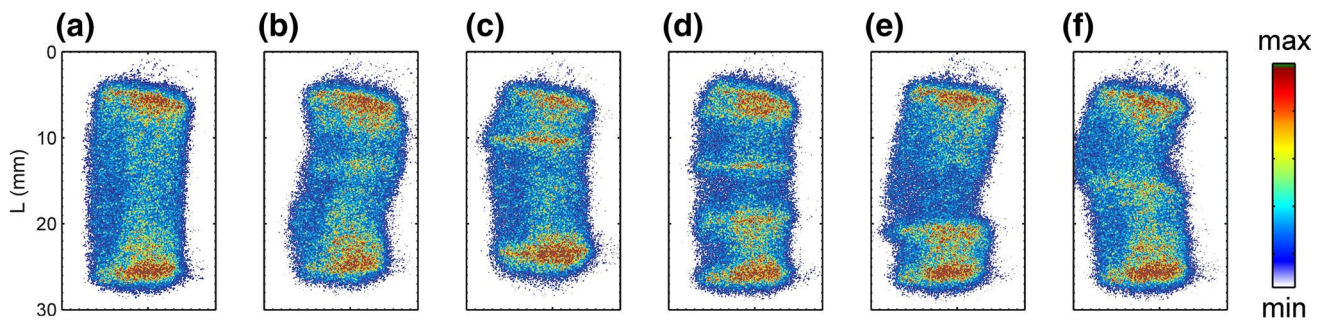


**Fig. 5** Examples of instantaneous beam profiles that have passed through **a** a turbulent air jet flow and **b–f** through a turbulent non-premixed  $C_2H_4$ /air flame of  $Re = 4330$  at  $x/d = 139$ . The images were

recorded at 2.2 m down-beam from the flame. A video recording 250 images can be found in *Media 1*

ES4020) without any optical filter. The CCD camera was synchronized with the ICCD camera for the LII to provide simultaneous measurement of the LII signals and the beam profiles.

To study the signal trapping, a 450-nm beam from a laser diode module (Oxxius Inc.) was employed to replace the LII laser beam. The round blue laser beam had a diameter of  $\sim 3$  mm and passed through the full width of the flames along the centreline. The blue laser beam was electronically modulated at  $50 \mu s$  in duration with a 5-Hz repetition. Part of the beam was reflected to a photodiode by a glass plate, and the laser power was recorded during measurement to correct for the fluctuations in laser power. The diffuse reflection from the diffuser was recorded by a CCD camera through a band-pass filter ( $450 \pm 5$  nm). It is noted that, for the turbulent flames and non-reacting flows and with the beam widening and flicking extensively, the transmitted beam was still located on the square diffuser. This allowed the reflection intensity on the whole diffuser to be integrated and the transmitted intensity of the laser beam to be determined.

### 3 Results and discussion

#### 3.1 Beam steering

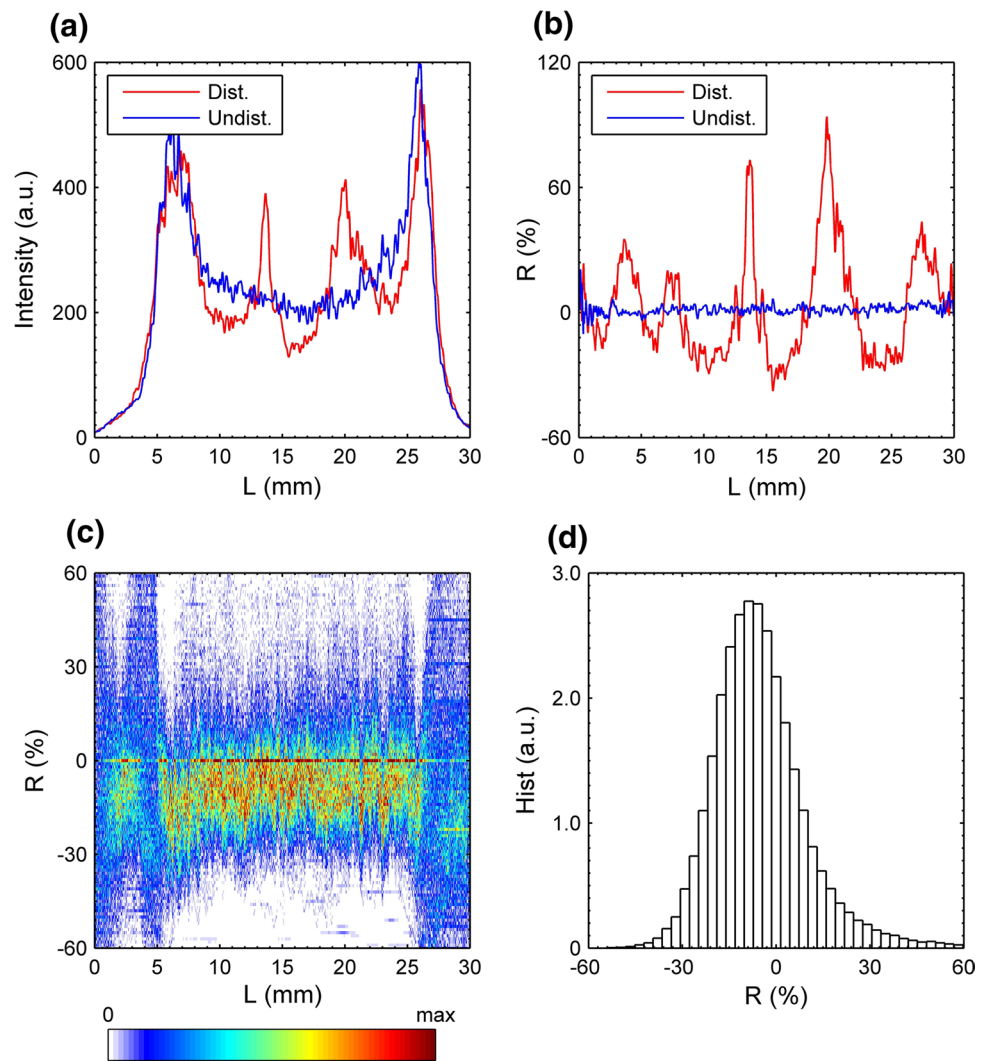
Figure 5 presents typical profiles of the laser beam for LII measurements after passing through an air jet flow (Fig. 5a) and a turbulent non-premixed  $C_2H_4$ /air sooting flame (Fig. 5b–f). The images were detected at a distance of 2.2 m down-beam from the flame. Additional sample of recorded beam profiles can be found in *Media 1*. The exit Reynolds number of the flame was 4330, and the laser beam was centred at  $x/d = 139$  downstream of the nozzle. Note that  $x$  is the distance above the jet exit and  $d$  is the internal nozzle diameter ( $d = 4.4$  mm). This height ( $x = 612$  mm) corresponds to the tip of the highly loaded soot zone, as shown

in Fig. 2b, c. It was found that for air jets at Reynolds number investigated, the beam profile was neither affected nor distorted, as shown in Fig. 5a. It should be noted that the width of the laser sheet ( $\sim 10$  mm) shown in Fig. 5 is much larger than that in the flames ( $\sim 600 \mu m$  undistorted) owing to the use of focussing optics.

The results shown in Fig. 5 and *Media 1* reveal that the turbulent flames severely deform and distort the beam spatial profile at  $x/d = 139$ , leading to a change in the laser fluence distribution. The intensities within laser beam vary significantly due to flame flicker both in the horizontal and in the vertical directions, even though the overall location of the beam does not change significantly; i.e. the direction of the laser sheet does not vary significantly (by  $< 130$  mrad). Importantly, effects of focussing in the vertical direction are very significant, which induces vertical redistributions of the laser fluence within the sheet, even though the changes in thickness in the horizontal direction (i.e. in sheet thickness) are less significant. Nevertheless, these flickering effects in the horizontal direction were found to be stronger in the downstream than in the upstream region of the turbulent sooting flame. It is worth noting that the beam profiles were recorded at a distance of 2.2 m down-beam from the flame because of the challenge of recording these profiles within the immediate vicinity of the flame due to the high soot loading and the infrared wavelength (1,064 nm) of the laser beam. While there may be some differences between the beam profiles within the flame and those recorded at the 2.2 m distance, it is still reasonable to use the beam profile at 2.2 m as a proxy to quantify the relative extent of beam distortions within flames.

Consistent with typical planar LII set-ups, the present laser sheet is focused horizontally to provide a thin measurement volume. Hence, the following analysis on the influence of fluence distribution is limited to the vertical direction. The fluence profile in this direction was calculated by integrating the signal along the radial direction of the beam. The result of this integration is shown in Fig. 6a,

**Fig. 6** **a** Axial profile of the intensities integrated in the radial direction of the beam for the disturbed (Fig. 5d) and the undisturbed (Fig. 5a) instantaneous beam sheets. **b** The intensity variation ratios  $R$  of the two curves shown in (a) relative to that of the average of 500 undisturbed beam sheets. **c** Statistics of the  $R$  values along the laser sheet height ( $L$ ) calculated from 500 laser shots. **d** The corresponding histogram of  $R$  values for the middle part of the laser sheet, i.e. from  $10 < L < 20$  mm as shown in (c)



which presents the integrated axial profiles from Fig. 5a, d. It is evident that the gradients in refractive index from the turbulent flame generate regions of both increased and decreased intensity of the laser fluence about the original values, especially over the range of  $10 < L < 25$  mm, where  $L$  expresses the distance from the image edge in the axial direction. The intensity variation ratio was employed to quantify the disturbance of the laser sheet and was defined as

$$R(I) = \left( \frac{I}{I_{\text{undist,averaged}}} - 1 \right) \times 100\%, \quad (7)$$

where  $I_{\text{undist,averaged}}$  is the intensity profile averaged from 500 undisturbed laser shots that were recorded in ambient air. Figure 6b presents the corresponding  $R$  values for the two curves as shown in Fig. 6a. It can be seen that the intensity fluctuations are very high for the disturbed beam, up to 80–90 %, while that of the undisturbed beam (for ambient air flows) is negligible.

Figure 6c presents the distribution of measured  $R$  values as a function of  $L$  calculated from 500 disturbed laser beams, while Fig. 6d presents the corresponding histogram of  $R$  over the region of  $10 < L < 20$  mm. This central flat region (for the undisturbed laser beams) is typically selected as being the most accurate for LII measurements and was also selected for the present work. In this region, the  $R$  value was measured to range mostly between  $-50$  and  $60$  %, while the peak of the histogram was found at  $R = -8$  % with a mean value of  $-4.7$  %. When the LII technique in a planar measurement is operated in the ‘plateau’ regime of the highly nonlinear fluence curve (e.g. as shown in Fig. 4), any decrease in the laser fluence to below the plateau region results in a strong decrease in the LII signal, while a similar increase in the laser fluence results in, at most, a small increase in the LII signal. This provides a potential explanation for the observation that the radial profiles in LII signals are frequently asymmetric in non-premixed jet flames [20, 21]. The laser sheets were

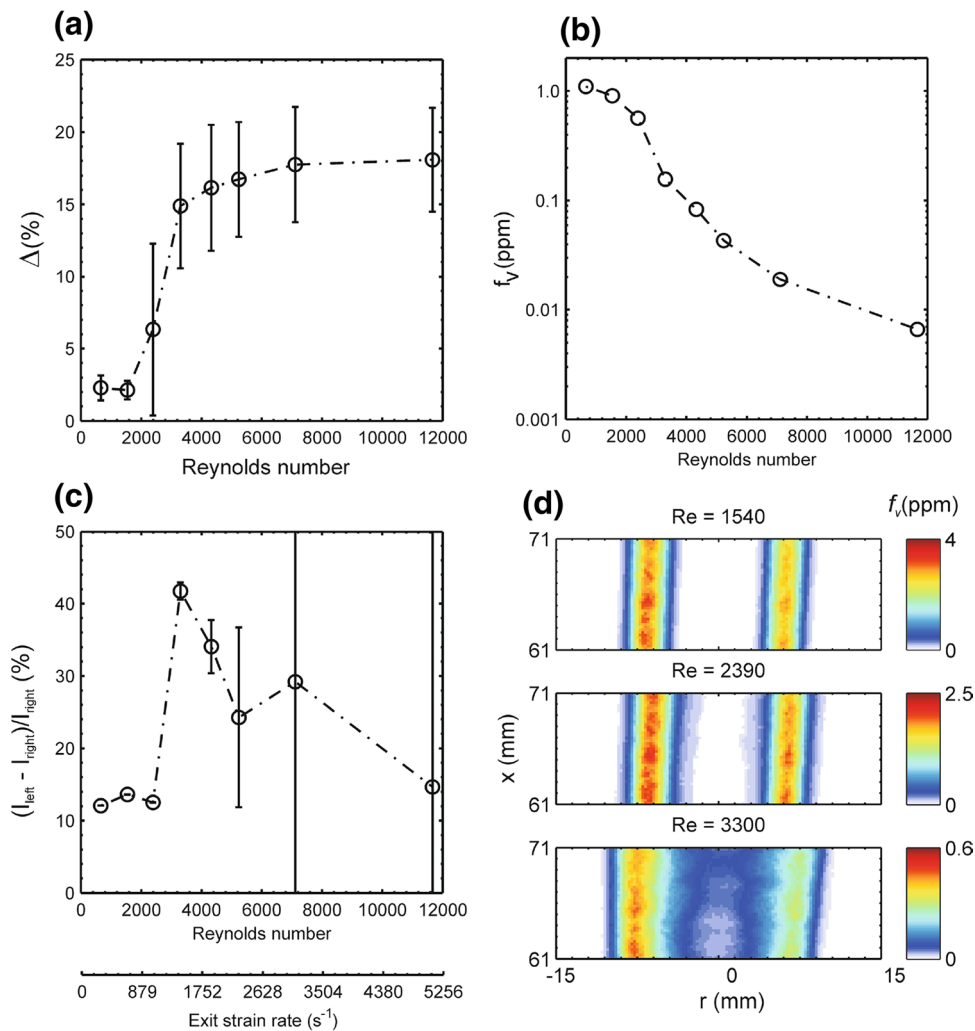


**Fig. 7** **a** Distortion extent of the beam sheet as a function of the exit Reynolds number in non-premixed  $\text{C}_2\text{H}_4/\text{air}$  sooting flames. The nozzle diameter was  $d = 4.4$  mm, and the measuring location was  $x/d = 15$ , i.e.  $x = 66$  mm. A parameter,  $\Delta$ , is introduced to quantify the distortion extent (see the main text for details). The results are calculated from 500 beam sheets recorded, and the error bars report the standard deviation of the  $\Delta$  values. **b** The mean soot volume fraction,  $f_v$ , calculated from 500 instantaneous LII images and averaged over a region from  $x = 61$  to 71 mm and over the full width of the

images. **c** The difference in the intensity of averaged LII signals from the left- and right-hand side of the flames. The *error bars* show the standard deviation of the differences in 500 instantaneous LII images. The exit strain rates corresponding to the Reynolds numbers labelled are shown as well. **d** The averaged LII images (have been converted to soot volume fractions) in three flames of different Reynolds numbers of 1540, 2390, and 3300, respectively. The laser beam passed the flames along the centerline from the left to the right of the images

distorted in the beam-incident side of the flames, which caused the LII signals generated by the disturbed laser fluence in the beam-exit side to be weaker than those in the beam-incident side generated by the undisturbed laser fluence. This effect should be significant when planar LII is performed in turbulent flames using a laser sheet without a homogenous spatial profile, e.g. a Gaussian profile laser sheet. Near the two wings the laser fluence must be below the ‘plateau’ regime or not fully saturated, even though the averaged laser fluence along the laser sheet thickness is in the ‘plateau’ regime. So, in these regions LII signals can decrease significantly when the laser sheet is distorted. This

further highlights the importance of the use of a laser sheet with good spatial profiles when LII is applied in turbulent flames diagnostics, as is already well accepted in studies performed in laminar flames to understand the LII process.

To quantify the extent of deformation to the intensity profiles of a laser sheet, the standard deviation of the  $R$  values was calculated. This can be expressed, for the  $j$ th laser shot recorded, as

$$\Delta(j) = \sqrt{\frac{\sum_1^n R_i^2}{(n-1)}}, \quad (8)$$

where the index  $i$  is the pixel number and  $n = 361$ , corresponding to the selected region from  $10 < L < 20$  mm.

Figure 7 presents the results of measurements performed in sooting flames of different Reynolds number at the exit of the nozzle with the aim of revealing the relationships between the  $\Delta$  value, the flame turbulence and the uneven intensity of LII signals. Here the exit Reynolds number was varied by varying the fuel gas velocity at the constant nozzle diameter ( $d = 4.4$  mm). The corresponding exit strain rates are shown in Fig. 7. The measuring location was constant at  $x/d = 15$ , i.e. 66 mm above the jet nozzle. Figure 7a presents the  $\Delta$  values as a function of the exit Reynolds number. The mean values of  $\Delta$  are calculated from 500 images of beam profiles, and the error bars present the standard deviations. Figure 7a indicates clearly that the deformity of the laser sheet is strongly dependent on the flame turbulence level. At this location, the flame with a  $Re = 1540$  did not induce any deformity to the laser sheet. Significant and intermittent laser sheet deformation can be observed at  $Re = 2390$  where the flame is in the transitional regime to turbulent flow. However, the extent of deformation increases markedly with only a small increase in the Reynolds number to  $Re = 3300$ , which is still transitional, but exhibits more significant temporal and spatial fluctuations in the flame sheet. This, in turn, causes significant spatial fluctuations in the laser sheet. Further increase to the Reynolds number did not make any significant difference to the  $\Delta$  value, which remains approximately constant over the range of  $6,000 < Re < 12,000$ .

Figure 7b presents the mean soot volume fractions calculated from 500 instantaneous LII images. The results were averaged over a region from  $x = 61$  to  $71$  mm and over the full width of the LII images. The reduction in  $f_v$  with increasing jet velocity is a result of the increased strain rate, as is well known [32–34]. Figure 7c presents the normalized differences between the averaged LII signal intensities (calculated from 500 images) on the left and right sides of the flame about the centreline, defined as  $(I_{\text{left}} - I_{\text{right}})/I_{\text{right}}$ . The LII signals were averaged for the full half-widths of LII images from  $x = 61$  to  $71$  mm, and the error bar presents the standard deviation of the differences calculated from 500 instantaneous LII images. A sharp increase in LII intensity difference from the  $Re = 2390$  flame to the  $Re = 3300$  flame was observed. Figure 7d presents examples of averaged LII images (have been converted to soot volume fractions) measured in three flames with  $Re = 1540$ ,  $2390$ , and  $3300$ , for which the laser beam direction is from the left to the right of the LII images. Significant asymmetry can be seen for the  $Re = 3300$  flame between the beam-incident (on the left) and the beam-exit side (on the right). The difference in signal is less significant for the other two flames of lower Reynolds numbers ( $Re = 1540$  and  $2390$ ). Combination of Fig. 7a, c reveals a strong correlation between the

$\Delta$  value and the LII signal difference. For an increase in the  $\Delta$  value from 5 % at  $Re = 2390$  to 15 % at  $Re = 3300$ , the normalized difference of the LII signals is increased markedly from 13 to 43 %; i.e. the measured soot volume fraction on the right side of the flame can be underestimated by up to 30 %. In Fig. 7c, the difference of ~12 % in the low Reynolds number flames corresponds to the low  $\Delta$  values of 4 % in Fig. 7a. This difference is attributed to the laser power extinction by the relatively high soot concentration in the low Reynolds number flames. When  $H_2$  blended into the  $C_2H_4$  flow to reduce the soot concentration to  $<0.6$  ppm in a set of laminar flames (with  $Re = 1900$ ), this difference is reduced to  $<3$  %. The drop in normalized difference in highly Reynolds number flames (but with the same  $\Delta$  value) is understood to be due to the decreased contribution of laser power extinction due to the low soot loading (see Fig. 7b). For the highly turbulent flames with  $Re = 7110$  and  $11,670$ , the soot sheets at this location ( $x/d = 15$ ) appear as isolated ‘islands’. This leads to the large error bars as shown in Fig. 7c.

The deformation of the laser sheet was found to vary with HAB both in non-reacting  $C_2H_4$  flows (Fig. 8a) and in  $C_2H_4$ /air sooting flames (Fig. 8b). As shown for the weakly turbulent flame with  $Re = 4330$  in Fig. 8b, the  $\Delta$  value was found to decrease from 22 to 5 % with an increase in HAB in the region of  $x/d < 50$ , and then to increase to 16 % in the region of  $x/d > 50$ . It is likely that the initial reduction is due to a decrease in effective Reynolds number because of the re-laminarization that occurs with combustion. This deduction is based on the measurements performed in the non-reacting  $C_2H_4$  flow, as shown in Fig. 8a, where the  $\Delta$  value was found to decrease monotonically with  $x/d$  as the fuel mixes more and more with the surrounding air. The increase in the  $\Delta$  value towards the tail of the flame is likely to be due to the increasing role of buoyancy-driven turbulent eddies. A similar trend in the  $\Delta$  value as a function of  $x/d$  was also found for other  $C_2H_4$ /air turbulent flames with different Reynolds numbers. It is worth emphasizing that significant beam steering is also found in the non-reacting  $C_2H_4$  flow, as is shown in Fig. 8a. The  $\Delta$  value can be up to 15–20 % in locations near the burner nozzle, e.g.  $x/d = 20$ . This degree of deformity level is about the same as that in the turbulent flames under study.

Figure 8c presents the difference of averaged LII signals on the two sides of the  $C_2H_4$ /air flames, which were measured simultaneously with the  $\Delta$  values as shown in Fig. 8b. There is no clear correlation between the  $\Delta$  value and the asymmetry of LII signals. Even a distorted beam with a low  $\Delta$  value, e.g. that at  $x/d = 60$  shown in Fig. 8b, can induce a significant asymmetry to LII signals. From Fig. 8c, a trend can be seen where the differences between the LII signals on the two sides are smaller for locations above  $x/d = 80$  and higher for those below  $x/d = 80$ . Around this



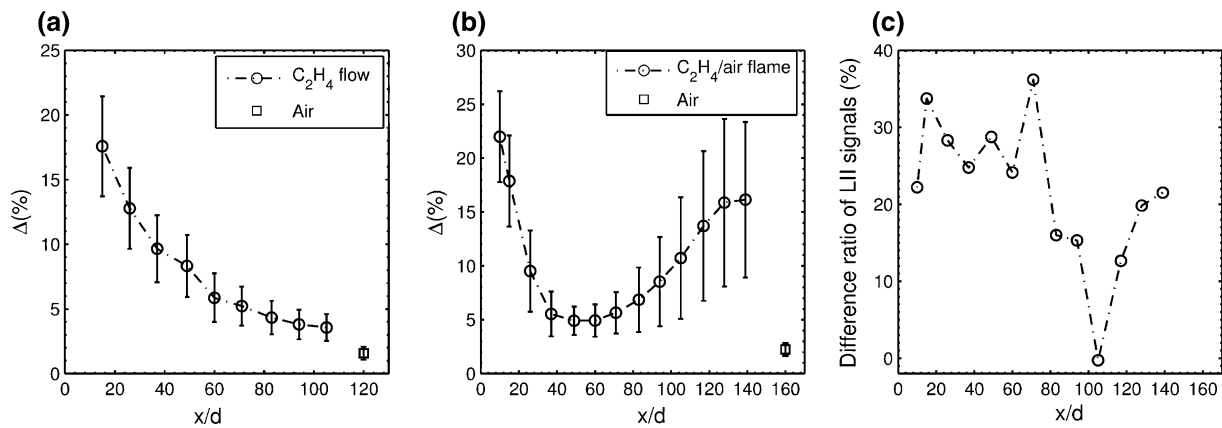
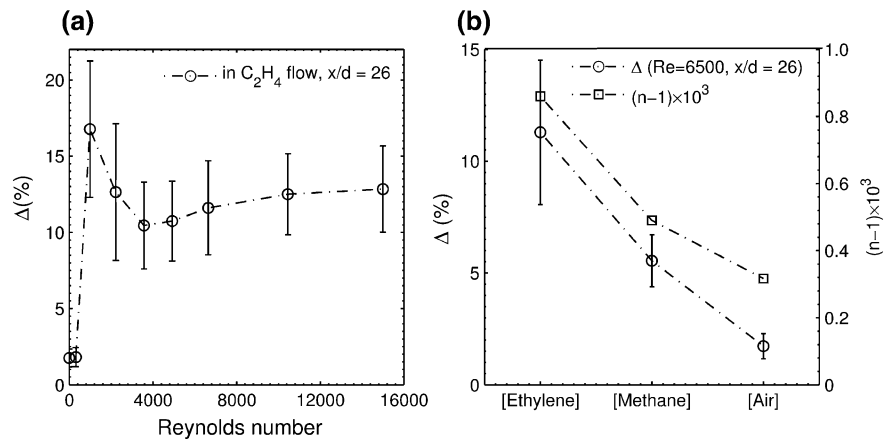


**Fig. 8** Intensity of beam steering as a function of the height above the burner nozzle that is denoted as  $x/d$  **a** in a non-reacting  $C_2H_4$  flow with  $Re = 6500$  with air co-flow and **b** in a  $C_2H_4$ /air sooting flame with  $Re = 4330$ . The intensities of beam steering measured in a tur-

bulent air flow are also shown (square). **c** The difference ratio of averaged LII signals on the two sides of the flame as a function of  $x/d$ , recording simultaneously with the beam profiles for calculating the results in (b)

**Fig. 9** **a** Intensity of beam steering as a function of the exit Reynolds number in non-reacting  $C_2H_4$  flows at  $x/d = 26$  and **b** in different gases with different refractive indices (also shown). The exit Reynolds number of the three non-reacting flows was kept to be 6500



location, i.e.  $x/d = 80$  ( $x = 352$  mm), the two soot layers merge together, which can be seen from the soot luminosity shown in Fig. 2b, where the flame has a similar Reynolds number of 5240. The trend that LII images become more symmetric in the downstream region was also demonstrated in a work of Köhler et al. [21].

Figure 9a presents the results of a further systematic measurement in a set of non-reacting  $C_2H_4$  flows with different Reynolds numbers. Because the  $C_2H_4$  gas has a relatively large refractive index, even a weakly turbulent flow with  $Re = 1000$  can induce strong beam steering and hence a large deformity to the beam. Moreover, as shown in Fig. 9a, the  $\Delta$  value is approximately constant as the  $Re$  number is increased above  $Re = 1000$ . In addition, Fig. 9b presents the  $\Delta$  values measured in the three turbulent non-reacting flows of ethylene, methane, and air with the same exit Reynolds number ( $Re = 6500$ ), as well as their refractive indices. It can be seen that the  $\Delta$  value is strongly

correlated with the refractive index, via the  $\frac{\partial K}{\partial x}$  dependence. Therefore, it is worth emphasizing that it is necessary to consider the influence of the refractive index on beam steering when optical methods are applied to turbulent flows/flames, even for non-reacting flows at room temperatures.

The present results also imply that beam steering will adversely impact on the accuracy of other quantitative measurements, in which planar optical methods are used. This applies, in particular, to techniques whose signals are critically dependent on the laser fluence. Such techniques include two-line atomic fluorescence (TLAF) thermometry [20, 35] and soot aggregate sizing by combining LII and elastic light scattering (LII + ELS) [36]. Potential methods with which to correct for beam steering effect include the use of Rayleigh imaging and ray tracing. However, while this has been demonstrated in particle-free flames [17], it is yet to be demonstrated in sooting flames. The application of a beam homogenizer [37] to shape the laser beam

before reaching the flame is one potential way to weaken the effects of beam steering. The collimated beam is modified into multiple beams that are emitted from micro lenses separately. In this way, the distortion of the total beam sheet, which is an average of the distorted sub-beams, has potential to be weakened and smoothed. However, its effectiveness in such applications is yet to be assessed. Additionally, a laser sheet not only with saturated fluence but also having a good spatial profile is beneficial for measuring soot volume fractions using planar LII in turbulent flames.

### 3.2 Signal trapping

The influence of signal trapping on LII measurements was investigated for an attached turbulent sooting flame on the same burner as introduced in the Sect. 2.2. The flame has a fuel mixture of  $C_2H_4/H_2/N_2$  with a composition of 40, 40, and 20 % by volume, respectively. The exit strain rate and the Reynolds number of the flame are  $12.95 \times 10^3 \text{ s}^{-1}$  and 15,000, respectively. Figure 10 presents the measured soot volume fractions using LII, as described in detail previously [20]. Briefly, LII signals around 430 nm were recorded in the turbulent flame and then calibrated by the LII signals recorded in a flat premixed  $C_2H_4$ /air on a McKenna burner. A continuous-wave laser beam at 1064 nm was used to perform extinction measurements in the flat flame. A value of  $K_e = 5.66$  was used to calculate the soot volume fractions, where  $K_e$  is the dimensionless extinction coefficient. The value of  $K_e = 5.66$  corresponds to  $E(m) = 0.3$  via  $K_e = 6\pi E(m)$ . It was assumed that the scattering contribution to beam extinction is negligible. The averaged soot volume fraction in this turbulent flame is up to 200 ppb and the maximum width of the averaged soot distribution is about 80 mm, at the same height. The combination of high soot loading and large flame width potentially causes LII signal trapping via soot absorption and scattering. In addition, PAH can also absorb LII signals in the blue spectral region [26, 38].

Figure 11a presents the measured attenuation of the 450 nm beam as a function of  $x/d$ . The laser beam has the wavelength close to that of the LII signal (430 nm) and passed through the whole flame along the centreline. The attenuation for the half-width of the flame was calculated by dividing the value for the full-width flame by two. This halved attenuation presents reasonably the time-averaged loss of LII signals at 450 nm emitted from the flame centreline. As shown in Fig. 11a, a maximum of 3 % has been found around  $x/d = 96$ , where the flame luminosity is widest and soot loading is highest (see Fig. 10). A 3 % signal loss might be reasonably considered as a negligible error source in measurements using LII. However, this soot loading is relatively light. Hence, it is still advisable to consider

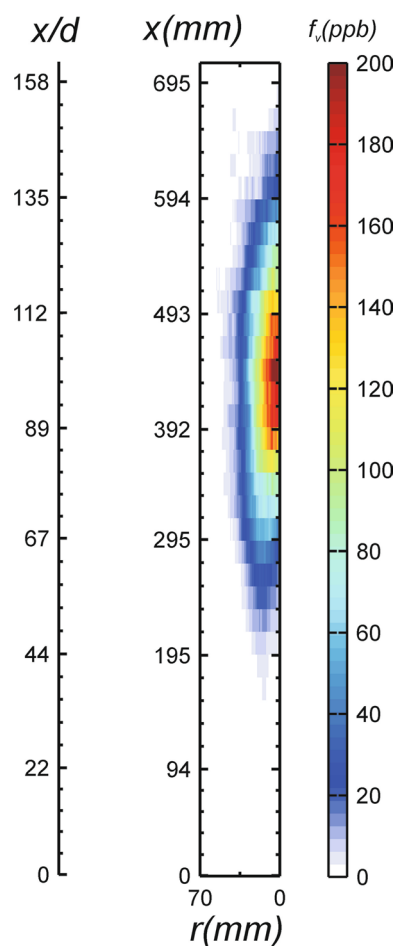


**Fig. 10** Averaged soot volume fractions measured in the ‘target’ flame using planar LII, replotted from a previous work [20]

this error source when LII is applied to high sooting flames and/or to large combustion systems. For example, the maximum signal loss reaches 6 % in a similar flame with a lower strain rate of  $3.95 \times 10^3 \text{ s}^{-1}$  and  $Re = 8,000$  (with  $d = 5.8 \text{ mm}$ ). In another study, a minimum transmission of approximately 0.88 in the half-width flame (i.e. a maximum signal loss of 12 %) of LII signals collected through the visible region was reported, at the middle height of an  $C_2H_4$  jet flame [39].

A comparison was also performed between the attenuation of signals at 450 nm based on the planar LII results and the line-of-sight extinction measurement. This comparison aims to assess the feasibility of estimating the magnitude of signal trapping directly from soot volume fractions measured with planar LII in a spatially symmetric system, like the jet flames in the present work. In calculating the attenuation based on the LII results shown in Fig. 10, the relation of  $\delta = 1 - e^{-K_e \cdot (f_v \cdot r) / \lambda}$  was used, where  $\delta$  denotes the attenuation,  $r$  is the radial distance,  $K_e = 5.66$ , and the wavelength  $\lambda = 450 \text{ nm}$ . The value of  $K_e$  is the same as

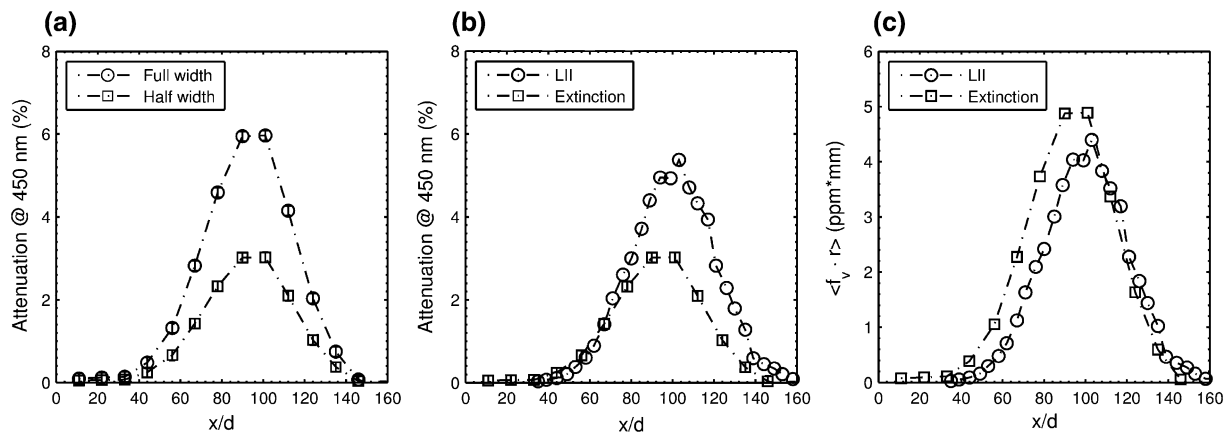


**Fig. 11** **a** Measured beam attenuation for both the full width (see Fig. 10) and the half width of the flame. **b** The signal attenuations for the half-width flame measured by line-of-sight extinction and cal-

culated based on the LII results in Fig. 10. **c** The radially integrated  $\langle f_v, r \rangle$  values measured via line-of-sight extinction and calculated based on the LII results, respectively

that used in LII signals calibration. Figure 11b presents the attenuations based on the two methods. Attenuation is overestimated based on the LII results above the middle of the flame, while a good agreement can be seen in the upstream region of the flame, but the magnitudes of attenuations are still in the same range, i.e. 3.2 and 5.6 % at the maximum, respectively. The difference is  $<2.5\%$  for all  $x/d$ . The consistency in the magnitudes of attenuation in the axial profiles implies that it is feasible to use LII signals to estimate and correct for the effect of signal trapping in mean soot volume fraction measurements.

The radially integrated values of  $\langle f_v, r \rangle$  are also compared. The same value of  $K_e = 5.66$  was used for the 450 nm beam in the calculations. Figure 11c presents the results from the two methods. Good agreement can be seen in the downstream region of the flame, i.e. above  $x/d = 100$ . Interestingly, at this height soot loading is highest, as shown in Figs. 9 and 11c. The  $\langle f_v, r \rangle$  curve measured via the blue beam extinction is biased towards the low  $x/d$ , which is likely due to the absorption of PAH around 450 nm. Another factor that can affect the accuracy and contribute to the difference in Fig. 11b, c is the uncertainty in the  $K_e$  value used in these calculations. Previous studies showed that the value of  $K_e$  varies significantly with the wavelength and the combustion condition [3, 27, 38].

The results in this part show that, in addition to soot volume fraction, signal trapping can also potentially affect the accuracy of other quantities that are measured via LII signals, such as soot particle temperatures that are measured by two-colour LII [24] and soot aggregate sizes that are measured by LII+ELS [36]. This influence does not apply for techniques where the signals are equally trapped, for example time-resolved LII (TiRe-LII) [40, 41]. To reduce the influence of signal trapping, detecting

LII signals at long wavelengths, e.g. around 700 nm, can potentially be used for cases where natural incandescence and PAH absorption are negligible. This is because of the  $\lambda^{-1}$  dependence of optical extinction of soot in the visible and near-infrared spectral regions [27]. Moreover, an online calibration method, i.e. performing simultaneous extinction measurements using a laser beam with the same colour as LII signals, can be beneficial for correcting signal trapping effects on mean data [10]. The use of large collection optics to reduce the effects of signal trapping in particle-laden flows had been identified by Kalt et al [42]. This technique, however, may not be suitable when soot sheets are continuous.

## 4 Conclusions

Both beam steering and signal trapping can result in a significant underestimate of soot volume fraction by planar LII measurements in atmospheric pressure turbulent sooting flames. In particular, the investigation has found that:

1. At atmospheric pressure, beam steering due to the gradients of the refractive index in turbulent flows can significantly alter the distribution of local fluence in a laser beam sheet, particularly in the axial direction of the flow. This occurs not only in high temperature turbulent flames but also in non-reacting cold flows such as in a turbulent  $C_2H_4$  jet issuing into air. Measured soot volume fraction can be underestimated by up to 30 % due to the nonlinear response of the LII signal to fluctuations in laser sheet intensity induced by beam steering. These fluctuations also explain the lack of symmetry in LII signals between the beam-

incident and the beam-exit sides of turbulent sooting flames, which have been observed previously but not explained. For this reason, measurements of  $f_v$  obtained from the beam-incident side are more reliable than those on the beam-exit side.

2. The significance of beam steering is strongly correlated with the extent to which a flow is turbulent, as characterized by the exit Reynolds number in the present work. The lower threshold of Reynolds number above which beam steering becomes significant was found to be approximately  $Re \sim 3300$  in a set of  $C_2H_4$ /air sooting flames on a jet nozzle ( $d = 4.4$  mm). Above this threshold, the extent of beam steering is insensitive to the exit Reynolds number. This threshold corresponds approximately to the transition from laminar to turbulence in a jet flow.
3. The extent of beam steering was found to be a function of the height above the burner nozzle, both in flames and in non-reacting flows. For the latter, beam steering was found to be strongly dependent on the refractive indices for the two studied gases methane and ethylene.
4. Due to signal trapping, LII signals in the blue spectral region can be attenuated by a few per cent in the regions of high soot loading within the studied flames. The magnitude of attenuation can be assessed reliably from planar LII results, but it is only possible to correct for the mean value of soot volume fractions.

Even though the present work has focused on the influences of the two effects on planar LII measurements, some of the conclusions are relevant to other optical methods, particularly techniques that are used for quantitative measurements, and are sensitive to laser fluence, for example, LII+ELS, two-colour LII, and TLAf that are frequently applied for measurements in sooting flames.

**Acknowledgments** The Australian Research Council (ARC) is gratefully acknowledged for their funding support. The authors wish to thank Dr Paul Medwell for useful discussions on the subject. The authors would like to thank the reviewers for their detailed comments and suggestions. Addressing these has strengthened the document significantly.

## References

1. K.C. Smyth, C.R. Shaddix, *Combust. Flame* **107**, 314–320 (1996)
2. S. De Iuliis, F. Migliorini, F. Cignoli, G. Zizak, *Appl. Phys. B* **83**, 397–402 (2006)
3. T.C. Williams, C.R. Shaddix, K.A. Jensen, J.M. Suo-Anttila, *Int. J. Heat Mass Transf.* **50**, 1616–1630 (2007)
4. X. Lopez-Yglesias, P.E. Schrader, H.A. Michelsen, *J. Aerosol Sci.* **75**, 43–64 (2014)
5. K. Kohse-Höinghaus, J.B. Jeffries, *Applied Combustion Diagnostics* (Taylor & Francis, New York, 2002)
6. H.A. Michelsen, *J. Chem. Phys.* **118**, 7012–7045 (2003)
7. C. Schulz, B.F. Kock, M. Hofmann, H. Michelsen, S. Will, B. Bougie, R. Suntz, G. Smallwood, *Appl. Phys. B* **83**, 333–354 (2006)
8. F. Goulay, P.E. Schrader, X. Lopez-Yglesias, H.A. Michelsen, *Appl. Phys. B* **112**, 287–306 (2013)
9. J.V. Pastor, J.M. Garcia, J.M. Pastor, J.E. Buitrago, *Meas. Sci. Technol.* **17**, 3279–3288 (2006)
10. J. Zerbs, K.P. Geigle, O. Lammel, J. Hader, R. Stirn, R. Hader, W. Meier, *Appl. Phys. B* **96**, 683–694 (2009)
11. R.L. Vander Wal, *Appl. Phys. B* **96**, 601–611 (2009)
12. B. Hemmerling, in *Proceedings SPIE Combustion Diagnostics*, vol. 3108, p. 32–37 (1997)
13. F. Weinberg, *Proc. Combust. Inst.* **26**, 939–944 (1996)
14. G. Magnotti, A.D. Cutler, P.M. Danehy, *Appl. Opt.* **51**, 4730–4741 (2012)
15. A. Stella, G. Guj, J. Kompenhans, M. Raffel, H. Richard, *Exp. Fluids* **30**, 167–180 (2001)
16. P.E. Dimotakis, H.J. Catrakis, D.C. Fourchette, *J. Fluid Mech.* **433**, 105–134 (2001)
17. S.A. Kaiser, J.H. Frank, M.B. Long, *Appl. Opt.* **44**, 6557–6564 (2005)
18. K.A. Thomson, M.R. Johnson, D.R. Snelling, G.J. Smallwood, *Appl. Opt.* **47**, 694–703 (2008)
19. M.P.B. Musculus, L.M. Pickett, *Combust. Flame* **141**, 371–391 (2005)
20. S.M. Mahmoud, G.J. Nathan, P.R. Medwell, B.B. Dally, Z.T. Alwahabi, *Proc. Combust. Inst.* **35**, 1931–1938 (2015)
21. M. Köhler, K.P. Geigle, W. Meier, B.M. Crosland, K.A. Thomson, G.J. Smallwood, *Appl. Phys. B* **104**, 409–425 (2011)
22. M. Wolfgang, *Flow Visualization*, 2nd edn. (Academic Press, Orlando, 1987)
23. M.Y. Choi, K.A. Jensen, *Combust. Flame* **112**, 485–491 (1998)
24. F. Liu, K.A. Thomson, G.J. Smallwood, *Appl. Phys. B* **96**, 671–682 (2009)
25. F. Migliorini, S. De Iuliis, F. Cignoli, G. Zizak, *Appl. Opt.* **45**, 7706–7711 (2006)
26. S. Bejaoui, X. Mercier, P. Desgroux, E. Therssen, *Combust. Flame* **161**, 2479–2491 (2014)
27. S.S. Krishnan, K.C. Lin, G.M. Faeth, *J. Heat Trans.-T. ASME* **123**, 331–339 (2001)
28. M. Köhler, K.-P. Geigle, T. Blacha, P. Gerlinger, W. Meier, *Combust. Flame* **159**, 2620–2635 (2012)
29. N.H. Qamar, Z.T. Alwahabi, Q.N. Chan, G.J. Nathan, D. Roekaerts, K.D. King, *Combust. Flame* **156**, 1339–1347 (2009)
30. C.R. Shaddix, J. Zhang, R.W. Schefer, in *Towards Quantitative Measurements of Soot Concentrations in Strongly Sooting Turbulent Jet Diffusion Flames*, in *Lasers, Sources and Related Photonic Devices*, OSA Technical Digest Series (Optical Society of America, 2010), paper LWB4. <http://www.opticsinfobase.org/abstract.cfm?URI=LACSEA-2010-LWB4>
31. H. Bladh, P.-E. Bengtsson, *Appl. Phys. B* **78**, 241–248 (2004)
32. V. Huijnen, A.V. Evlampiev, L.M.T. Somers, R.S.G. Baert, L.P.H. de Goeij, *Combust. Sci. Technol.* **182**, 103–123 (2010)
33. M.E. Decroix, W.L. Roberts, *Combust. Sci. Technol.* **160**, 165–189 (2000)
34. H. Wang, D.X. Du, C.J. Sung, C.K. Law, *Proc. Combust. Inst.* **26**, 2359–2368 (1996)
35. C.F. Kaminski, J. Engstrom, M. Aldén, *Proc. Combust. Inst.* **27**, 85–93 (1998)
36. J. Reimann, S.A. Kuhlmann, S. Will, *Appl. Phys. B* **96**, 583–592 (2009)
37. S. Pfadler, F. Beyrau, M. Löffler, A. Leipertz, *Opt. Express* **14**, 10171–10180 (2006)
38. F. Migliorini, K.A. Thomson, G.J. Smallwood, *Appl. Phys. B* **104**, 273–283 (2011)

39. C.R. Shaddix, J.Y. Zhang, R.W. Schefer, J. Doom, J.C. Oefel-  
ein, S. Kook, L.M. Pickett, H. Wang, *Understanding and pre-  
dicting soot generation in turbulent non-premixed jet flames*,  
SAND2010-7178, Sandia National Laboratories, (2010)
40. Z.W. Sun, D.H. Gu, G.J. Nathan, Z.T. Alwahabi, B.B. Dally,  
Proc. Combust. Inst. **35**, 3673–3680 (2015)
41. R. Hedef, K. Geigle, J. Zerbs, R. Sawchuk, D. Snelling, Appl.  
Phys. B **112**, 395–408 (2013)
42. P.A.M. Kalt, C.H. Birzer, G.J. Nathan, Appl. Opt. **46**, 5823–5834  
(2007)